Mechanochemical synthesis and structural characterization of gallium sulfide Ga2S3

Killian Denoue, François Cheviré, Christophe Calers, Louisiane Verger, David Le Coq, Laurent Calvez

Mechanochemical synthesis and structural characterization of gallium sulfide Ga_2S_3

Killian DÉNOUE[1], François CHEVIRÉ[1], Christophe CALERS[1], Louisiane VERGER[1], David LE COQ[1], Laurent CALVEZ[1]**

[1] Univ Rennes, CNRS, ISCR (Institut des Sciences Chimiques de Rennes) - UMR 6226, F-35000 Rennes, France

*louisiane.verger@univ-rennes1.fr, laurent.calvez@univ-rennes1.fr

ABSTRACT

Crystalline gallium (III) sulfide Ga_2S_3 samples have been prepared by mechanical-alloying instead of usual heating process. A safe, energy-efficient, and fast process of only 4 hours of mechanosynthesis led to the formation of polycrystalline Ga_2S_3 from pure Ga and S as raw materials. X-ray diffraction measurements and Rietveld refinements show that the as-prepared material is a mixture of mainly hexagonal wurtzite-type β-phase (68 ± 5 wt%; space group $P6_3mc$ (No. 186)) along with some cubic sphalerite-type γ-phase (32 ± 5 wt%; space group $F\text{-}43m$ (No. 216)). *In situ* high-temperature X-ray diffraction measurements show that the monoclinic phase (space group *Cc* (No. 9)) appears at 450°C. Scanning electron microscopy analyses reveal that the morphology of the powder is characterized by aggregates of nanometric

particles. Their sizes measured by laser diffraction show a median size around 170 nm after 4 hours of ball-milling.

KEYWORDS

Gallium sulfide; Mechanochemical synthesis; X-ray diffraction; Chalcogenide

1. Introduction

Gallium (III) sulfide (Ga_2S_3) is a semiconducting material with attractive properties for a large number of applications. Ga_2S_3 combined with other compounds is used as anode materials as well as for solid-state electrolytes in Li-ion and Na-ion batteries to improve the cyclability and the stability of the electrodes thanks to its self-healing properties [1-5]. Moreover, luminescence properties can be achieved either by using nanocrystalline Ga_2S_3 quantum dots [6] or by doping Ga_2S_3-based chalcogenide glasses with rare-earth [7,8] for light emission or fluorescence applications. When associated with lanthanum, the synthesized glasses possess excellent manufacturing properties to design optical lenses, optical amplifiers, laser optical elements used in telecommunications and sensors [9,11]. Ga_2S_3 can also be associated with germanium sulfide and halides or iodides, to obtain chalcogenide glasses and glass-ceramics presenting non-linear optical properties such as second and third harmonic generation [12-15]. Finally, Ga_2S_3 is used for its semiconductor properties in the fields of microwave frequencies [16, 17], photo-detection [18, 19], and as a precursor for solar panels [20] and for photo-catalysis to generate hydrogen from water splitting [21].

Four different crystallographic forms of Ga_2S_3 have been reported in the literature [22-27]. Hexagonal β-Ga_2S_3 crystallizes in the $P6_3mc$ space group, in a wurtzite-type structure (**Figure**

1 a). Ga atoms are statistically distributed with an occupation of 2/3 on the 2b site of the lattice and are located on tetrahedral sites formed by S, with Ga-S bonds almost equivalent (3 at 2.254 Å and 1 at 2.268 Å). Hexagonal α-Ga_2S_3 (space group $P6_1$) is a superstructure of the β wurtzite-type phase. They differ by a partial ordering of the Ga atoms. In the α structure, Ga atoms can occupy 3 different sites, but only partially because the anionic network is the same as the wurtzite structure. Pardo *et al.* [28] showed that while one site is fully occupied, the other 2 are randomly occupied. This phase was not identified in our work by X-ray diffraction (XRD) characterizations and is not further discussed. Monoclinic α'-Ga_2S_3 (space group *Cc*) is also a superstructure of the wurtzite, but in this case a full ordering between vacancies and Ga atoms in the cationic network is observed (**Figure 1 b**). Ga is still in a tetrahedral environment characterized by 3 Ga-S bonds almost equivalent (around 2.31 Å) and a shorter one (around 2.20 Å). S atoms exhibit 2 distinct environments as shown in **Figure 1 b**: while S1 and S3 are surrounded by 3 Ga atoms with a Ga-S distances around 2.31 Å, S2 is linked to only 2 Ga with much shorter Ga-S bonds at 2.20 Å. Finally, a cubic sphalerite-type structure is also reported for γ-Ga_2S_3, (space group *F*-43*m*) with a random distribution of vacancies and Ga atoms on the cationic sites with an occupation of 2/3 and at the center of tetrahedra formed by S with Ga-S at 2.258 Å (**Figure 1 c**).

Synthesis of Ga_2S_3 with a control of polymorphism and stoichiometry remains a challenge. While monoclinic α'-Ga_2S_3 is exactly stochiometric, the other polymorphs exhibit a sulfur deficiency [27]. Various techniques have been reported to synthesize crystalline bulk Ga_2S_3. It was initially obtained by reacting Ga and S in sealed silica tube at temperature above 1000°C. The monoclinic α' form can be synthesized this way and is stable from room temperature to melting. By controlling the Ga/S ratio introduced and the quenching temperature, the other

polymorphs can also be obtained [27-31, 33]. A reaction involving sulfur vapors on metallic gallium at 1250 °C has been demonstrated by Brukl et al. [32]. The most common reported synthesis is the treatment at 750 °C of gallium (oxo)hydroxides, GaO(OH) or $Ga(OH)_3$, under flowing H_2S [26,27,28]. Only the α'-Ga_2S_3 polymorph is formed by this technique. The flammability of H_2S gas brings safety concerns. Furthermore, all the bulk syntheses mentioned above are unsafe due to possible explosion hazard at the temperatures used caused by the high vapor pressures of sulfur involved. Recently, three safer processes have been described in the literature: (i) a green synthesis involving the reaction of $GaCl_3$ and Na_2SO_4 in aqueous solution leading to the formation of nanoparticles of α-Ga_2S_3 [34], (ii) thermal decomposition of gallium xanthate precursors to obtain γ-Ga_2S_3 [35] and (iii) a mechanical milling approach starting from metallic gallium and sulfur [36].

Mechanochemical synthesis is a technique used more and more recently to produce unique materials. It combines several advantages. From a processing point of view, it is a simple, rapid, no-waste and energy-efficient pathway compared to other methods. It also offers the possibilities to synthesize materials without solvent or gas, and to obtain metastable phases or materials that usually require high temperatures. It is also a top-down approach to produce nanoparticles [37]. Mechanochemical processes find multiple applications from the synthesis of semiconductor materials [38], to the treatment of wastes such as metallurgical residues [39], leaded glasses [40], through catalysis, cosmetics and the medical field [41]. Finally, a large number of chalcogenides have already been produced using this synthesis method, ranging from binary to quaternary [42,43]. This technique was chosen to carry out this work.

In the present study, we investigate the synthesis of crystalline Ga_2S_3 by mechanochemical technique from pure Ga and S as raw materials. The as-prepared crystalline powder is

characterized by a laser diffraction particle sizer and a scanning electron microscope (SEM) and its crystalline forms are determined by the means of XRD analyses and Rietveld refinements.

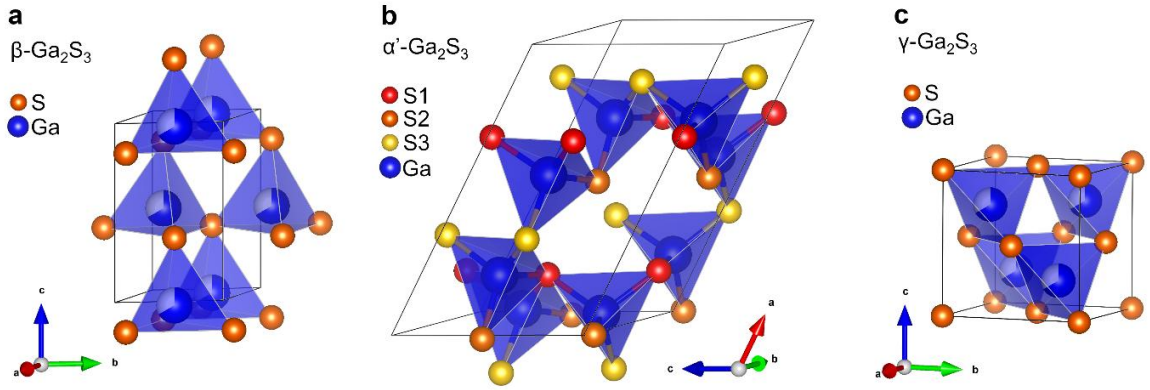

Figure 1. Crystal structures of the different polymorphs of Ga_2S_3: (a) hexagonal β phase (space group $P6_3mc$) [25], (b) monoclinic α' phase (space group Cc) [26], and (c) cubic γ phase (space group F-43m) [22]. Gallium atoms are represented in blue, sulfur atoms are represented in yellow, orange or red.

2. Experimental section

2.1. Synthesis

Ga_2S_3 was prepared by mechanochemical synthesis using a planetary ball mill (Fritsch, Pulverisette 7). 8 g of stoichiometric proportions of gallium (Neyco, 99.99%) and sulfur (Strem Chemical Inc., 99.999%) was placed into a tungsten carbide (WC) vessel (internal volume of 45 mL) with 10 WC balls (10 mm in diameter) resulting in balls to powder mass ratio of 10:1. The mechanochemical reaction was performed from 1 to 10 hours at a fix rotation speed of 400 rpm. The vessel was opened every hour to scrub and hand grind the powder stuck to the walls in order to obtain a uniform powder. All processes were performed in a dry N_2 atmosphere.

2.2. Characterization techniques

XRD measurements were performed at room temperature on samples protected from air by a Kapton (polyimide) window to avoid moisture corrosion of fine submicron particles. They were recorded in the 10- 90° 2θ range with a 0.0261° step size with each data point having an effective total counting time of 40 s/step using a PANalytical X'Pert Pro diffractometer (Cu $K_{\alpha1}$, $K_{\alpha2}$ radiations, $\lambda_{K\alpha1}$ = 1.54056 Å, $\lambda_{K\alpha2}$ = 1.54439 Å, 40 kV, 40 mA, PIXcel 1D detector). Data collector and HighScore Plus software were used for recording and analysis of the patterns, respectively. The powder XRD patterns for Rietveld refinements were collected in the 2θ 10- 120° range with a 0.026° step size with each data point having an effective total counting time of 400 s/step. All calculations were carried out using Fullprof and WinPlotr programs [44, 45]. High temperature XRD patterns were acquired from room temperature up to 800°C with a step of 50°C (rate: 5°C/min) under a flowing nitrogen atmosphere in the 10-90° 2θ range with a 0.026° step size with each data point having an effective total counting time of 40 s/step using a PANalytical Empyrean diffractometer (Cu $K_{\alpha1}$, $K_{\alpha2}$ radiations, $\lambda_{K\alpha1}$ = 1.54056 Å, $\lambda_{K\alpha2}$ = 1.54439 Å, 40 kV,40 mA, PIXcel 3D detector) equipped with an Anton Paar HTK1200 temperature chamber.

Laser grain size measurements were performed on Fritsch, Laser particle sizer Analysette 22 NanoTec, using a wet dispersion unit, after different milling times.

SEM images were obtained on JEOL JSM-IT 300 using an acceleration voltage of 15 kV and a magnification x5000.

3. Results and discussion

As shown in **Figure 2**, the color of the powders evolves from brown to yellow as a function of milling time. These color changes indicate the gradual disappearance of raw elements due to their progressive reaction to form Ga_2S_3. **Figure 2** also shows the XRD patterns acquired on the powder after different milling times between 1 h and 4 h. The presence of both a diffraction halo, located between 15 and 25 ° 2θ, and the background drift are due to the Kapton window. After only 1 h of mechanical milling (black diagram in **Figure 2**), monoclinic α'-Ga_2S_3 (*Cc*, JCPDS no. 01-076-0752) is detected. The two diffraction peaks at 16.654 and 18.613 ° 2θ is an evidence for the presence of this polymorph, as they are not present in the α, β or γ form. However, their low relative intensity compared to the main characteristic peak of Ga_2S_3 can be explained by the presence of β (*P*6$_3$*mc*, JCPDS no. 01-084-1441) and γ (*F*-43*m*, JCPDS no. 00-043-0916) polymorphs as well, since their diffraction peaks are overlaid with the α' polymorph (see the Bragg positions in **Figure 2**). GaS (*P*6$_3$*/mmc*, JCPDS no. 01-074-0227) is also detected as a minority phase. The presence of GaS can explain the color of the powder. After 2 h of milling (red diagram in **Figure 2**), GaS diffraction peaks intensity decreases and they disappear after 3 h of milling (blue diagram in **Figure 2**). At the same time, some broadening and an evolution of the Ga_2S_3 diffraction peaks are observed. The former point indicates a reduction of the crystallites size during prolongated ball milling. The latter suggests a structural modification of the Ga_2S_3 phase. Firstly, the two low intensity peaks around 20 ° 2θ characteristic of α'-Ga_2S_3 are not detected after 3 h and 4 h of milling time. An XRD acquisition of the powder after 4 h of milling time without the Kapton window was done for the high temperature study and also show the absence of these two peaks (**Figure 6** bottom pattern). Secondly, the relative intensity of the peaks at 29.6, 49.4 and 58.7° 2θ noticeably increases compared to the other peaks. These two modifications can be explained by a reaction of the monoclinic α'-Ga_2S_3 phase with GaS to form

a mixture of hexagonal β- and cubic γ-Ga_2S_3. The intensity of the peaks aforementioned is the result of the contribution of the (002), (110) and (112) lines indexed in the *P6₃mc* space group of the β phase, together with the (111), (220) and (311) lines indexed in the *F-43m* group of the γ phase, as illustrated on **Figure 2** with the Bragg position of the β- and γ-Ga_2S_3 polymorphs. To summarize at this point, reaction between Ga and S takes place within 1 h of milling, leading to a mixture of different polymorphs of Ga_2S_3 and GaS, which further react to form a mixture of β and γ-Ga_2S_3 after 4 h of milling.

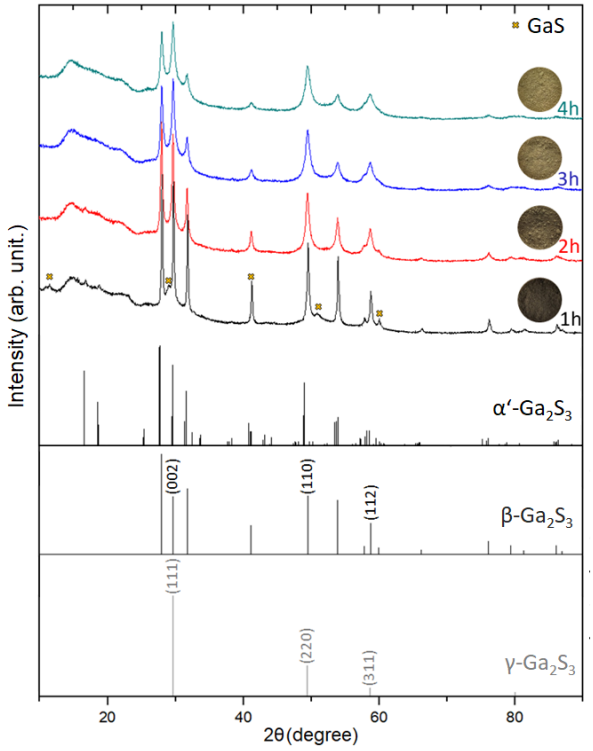

Figure 2. XRD diagrams of Ga_2S_3 samples prepared by ball milling for different periods (from bottom to top: 1 h, 2 h, 3 h and 4 h) with associated photographs. The three lowermost diagrams represent the peaks position of monoclinic α'- Ga_2S_3 (JCPDS no. 01-076-0752), hexagonal β-Ga_2S_3 (JCPDS no. 01-084-1441) and cubic γ-Ga_2S_3 (JCPDS no. 00-043-0916).

Rietveld refinements were carried out to confirm and quantify the relative amount of these two polymorphic species of Ga_2S_3 after 4 h of milling. As illustrated in **Figure 3**, the diffraction peaks show a substantial half-height width, which can influence the refinement parameters. This observation occurs for crystalline compounds obtained by mechanochemistry since their particle size is definitively smaller comparatively to the particle size of compounds obtained by other techniques [37]. According to the refinements, a quantitative estimation shows that the hexagonal β phase represents 68 wt% (±5%) of the crystallized mixture and the remaining 32 wt% (±5%) are the cubic γ phase. After 4 h of milling, it is clearly shown that the experimental data and the refinements are much better when both hexagonal and cubic phases are included (**Figure 3 b**), comparatively to the refinement with only the hexagonal phase (**Figure 3 a**). Preferential orientation and morphology anisotropy of nanocrystals can typically result in a modification of the relative intensity and width of diffraction peaks. However, this effect in our case can be excluded as mechanical milling results in the formation of isotropic particles with no preferential orientation as shown latter by SEM. Kristl *et al.* also used mechanochemistry to synthesis Ga_2S_3 [36]. Milling conditions are different than this work, they used stainless steel vessel with balls to powder mass ratio of 20:1. After 2 h of milling time, they obtained a material with a similar XRD pattern than the powder obtained in this work after 4 h. The condition used here are then milder than Kristl *et al*. Although they identify their material to be β single-phase [36], they rather probably have a mixture of β and γ polymorphs like evidenced in this paper.

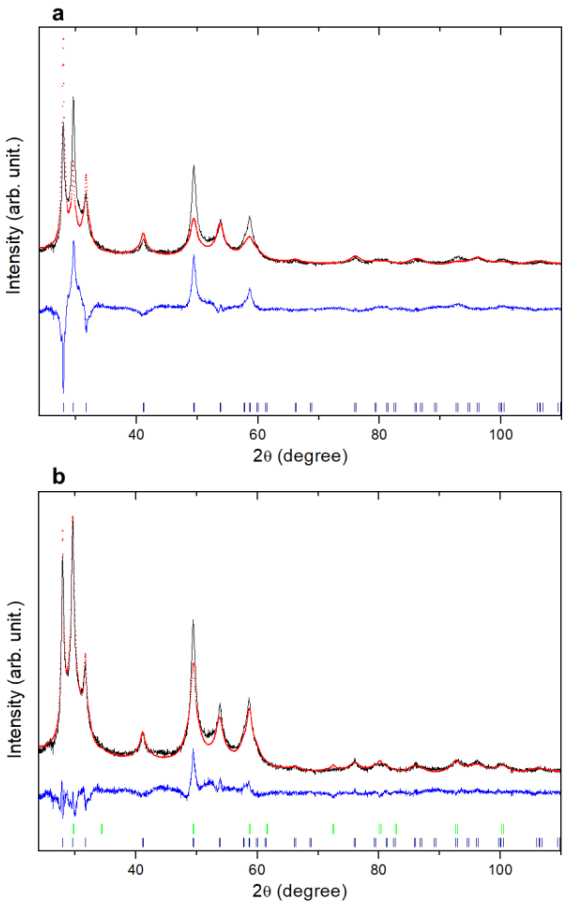

Figure 3. Rietveld refinement (black line) of Ga_2S_3 synthesized by mechanical milling for 4 h (red dots) considering (a) only the hexagonal β-Ga_2S_3 phase (JCPDS no. 01-084-1441) and (b) the hexagonal β-Ga_2S_3 phase (JCPDS no. 01-084-1441) and cubic γ-Ga_2S_3 phase (JCPDS no. 00-043-0916). The blue lines plot the difference between observed and calculated intensities. Green and blue bars show the position of the Bragg reflections for γ-Ga_2S_3 and β-Ga_2S_3, respectively.

As mentioned in the introduction, only α'-Ga_2S_3 is stoichiometric and stable, the other polymorphs showing an S deficiency. This is especially true for γ-Ga_2S_3 which is the furthest apart from the ideal composition Ga_2S_3 in the binary Ga-S: its theoretical composition is reported

to be close to $Ga_2S_{2.76}$ [22] (see binary diagram in [33]). Pardo *et al*. have reported that an annealing treatment on β-Ga_2S_3 results in the decomposition of the compound into α'-Ga_2S_3 and GaS [33]. Besides, by heating a mixture of different amount of GaS and α'-Ga_2S_3, they also showed that γ-Ga_2S_3 can be obtained together with one of the initial reactants. These results are consistent with the reactivity put forward in our study: after the formation of the two stable compounds α'-Ga_2S_3 and GaS, mechanical milling enables the formation of substoichiometric polymorphs, β and γ. The presence of both the hexagonal and cubic phases of Ga_2S_3 is not surprising since their structure is based on the occupancy of almost identical tetrahedral sites by Ga, with different atomic stacking (ABAB for β and ABCABC for γ) (**Figure 1**). Furthermore, γ-Ga_2S_3 is always found in the presence of other polymorphs, and has only been isolated as a powder very recently by thermolysis of gallium xanthate precursors [35]. The conditions involved in the high-energy mechanical milling seem to promote the synthesis of metastable polymorphs of Ga_2S_3 (β and γ) which can only be obtained by specific heating and quenching temperature by traditional high temperature synthesis.

Interestingly, the formation of GaS during the first hour of mechanical synthesis instead of pure Ga_2S_3 means that probably a certain amount of S becomes poorly crystallized and not detected by XRD. To investigate further the influence of the initial S amount on the resulting phases obtained, two synthesis were tested with a 5 % molar excess of S, and 9 % molar default of S. The precursors were mechanically milled during 4 h, as described in the experimental section. **Figure 4 a** and **Figure 4 b** show Rietveld refinements of XRD patterns acquired on powders obtained with 9 % molar default of S and 5 % molar excess of S, respectively. The intensity of the (111), (220) and (311) peaks indexed in the space group of γ-Ga_2S_3 remains

constant while the intensity of the other peaks increases with an excess of S. The sample synthesized with a 5 % molar excess of S is composed of 24.6 wt% of γ-Ga_2S_3 and 75.4 wt% β-Ga_2S_3 (±5%), while the sample obtained with a 9 % molar default of S is composed of 41.9 wt% of γ-Ga_2S_3 and 58.1 wt% β-Ga_2S_3 (±5%). The formation of the cubic γ-phase is then promoted by a S deficiency, which is consistent with the fact that this polymorph is the furthest apart from the ideal composition.

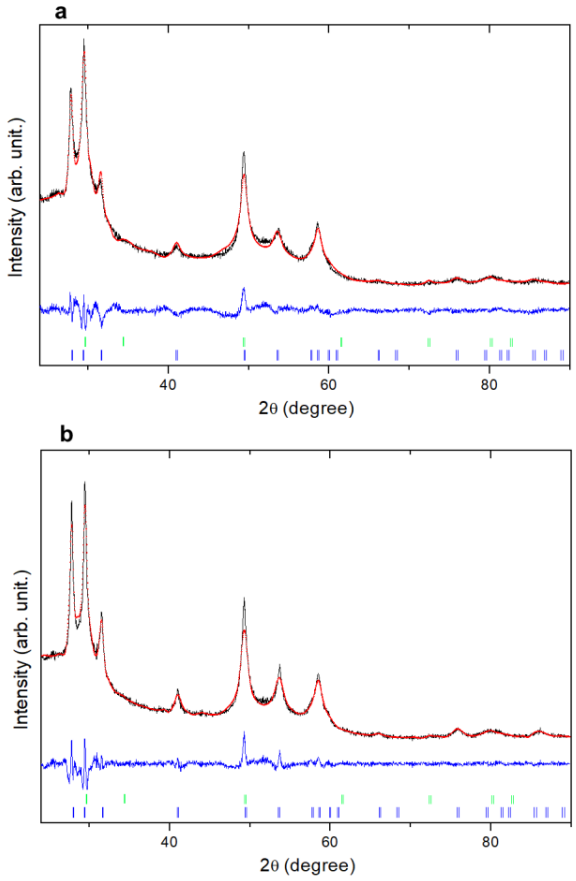

Figure 4. Rietveld refinement (black line) of Ga_2S_3 samples prepared by ball milling with 9 % molar default (**a**) and 5% molar excess of S (**b**). The blue lines plot the difference between observed and calculated intensities. Green and blue bars show the position of the Bragg reflections for γ-Ga_2S_3 and β-Ga_2S_3, respectively.

When Ga and S are introduced in stoichiometric proportion, the milling time was extended up to 10 h to investigate a possible evolution of the phases. There was no obvious difference between the XRD patterns of Ga_2S_3 powders after 4h and 10h of grinding (not shown). In addition, as underlined previously, the evolution of the powder color is very marked from 1 h to 4 h, but it remains similar after 10 h. These two observations are consistent with the formation of the final mixture of the 2 Ga_2S_3 polymorphs after 4 h of mechanical milling.

Nevertheless, some evolutions can still be pointed out as depicted in **Figure 5 a** in which the morphology of the Ga_2S_3 powder after 4 h and 10 h of mechanosynthesis is presented. This powder is composed of aggregates of different sizes (micron scale), themselves composed of spherical particles of submicron sizes. A diminution of the average grain size is visible when comparing the SEM photographs after 4 h and 10 h. To quantify this observation, the median grain size (Q50) of the powder was measured by laser particle sizer after different grinding time. As shown both in **Figure 5 b**, the Q50 exponentially decreases as a function of grinding time from 420 nm down to 42 nm for 1 h and 10 h, respectively. Kristl *et al.* [36] also obtained aggregates of spherical particles. However, using their conditions 2 h is enough to decrease the diameter of the particles down to 40 nm. As previously observed when comparing the XRD pattern, the condition used in this work are then milder. Although no further modification of the structure of Ga_2S_3 is observed after 4 h based on the XRD patterns, the previous analyze clearly evidences that it is possible to control and reduce the particle size of the compound by extending the grinding time. Controlling the grain size of Ga_2S_3 as a precursor is crucial depending on the subsequent reaction or application.

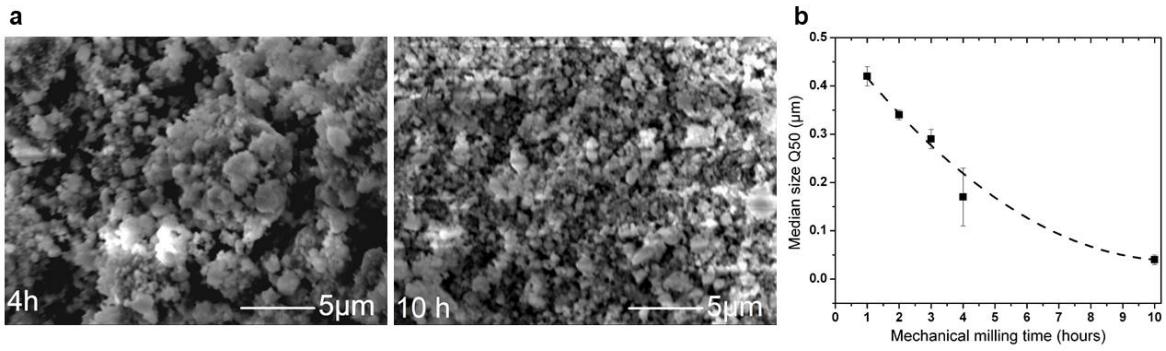

Figure 5. (a) SEM images of Ga_2S_3 powder after 4 h (left) and 10 h (right) of mechanosynthesis (accelerating voltage: 15 kV, magnification: x 5000). (b) Evolution of the median size Q50 from 1 hours up to 10 hours determined by laser particle sizer.

In situ high temperature XRD measurements were carried out to investigate the stability in temperature of Ga_2S_3 powders obtained after 4 h of milling time. **Figure 6** shows the evolution of the XRD patterns acquired at room temperature, and then every 50°C from 50°C up to 800°C. A phase transition is observed starting at 450°C, from the mixture of the two polymorphs β and γ-Ga_2S_3 to monoclinic α'-Ga_2S_3 (*Cc*, JCPDS no. 01-076-0752). The latter is stable and continuously crystallizes up to 800 °C. Differential scanning calorimetry (DSC) was conducted on Ga_2S_3 powders after 4 h of milling time. An exotherm was detected around 410°C, that coincide with the formation of α'-Ga_2S_3 evidenced in the high temperature XRD data. No predominance of one of the two preliminary phases over the other is observed before the transition to the α'-phase. The XRD diagram acquired on the powder at room temperature after the *in situ* experiment shows that only the monoclinic phase is still present (blue pattern in **Figure 7**) meaning that the phase transition observed upon heating is then irreversible. This is consistent with the fact that β and γ are metastable polymorphs of Ga_2S_3. α'-Ga_2S_3 is

stoichiometric, meaning that a loss of Ga should be observed together with the decomposition of substoichiometric β and γ phases. Indeed, the presence of supplementary peaks attributed to monoclinic Ga_2O_3 phase (JCPDS no. 00-041-1103), show that the excess of Ga reacts with some oxygen contamination, probably coming from handling the sample shortly in air during the setup of the experiment or from the nitrogen atmosphere.

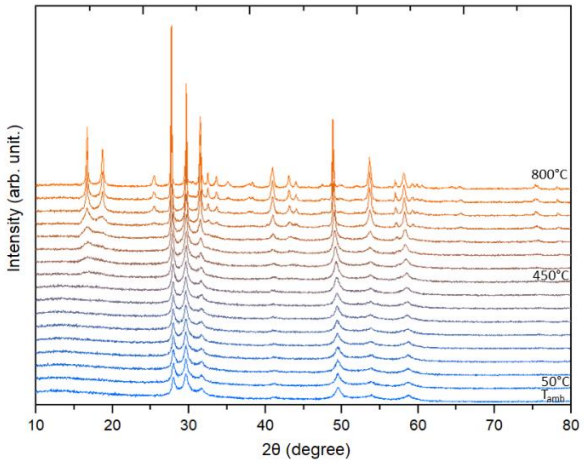

Figure 6. *In situ* high temperature XRD patterns of the Ga_2S_3 sample obtained after 4 h of milling time, from 50°C to 800°C every 50°C.

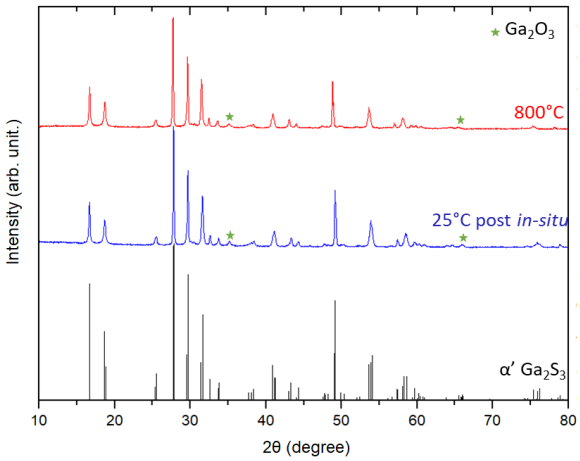

Figure 7. Comparison between XRD patterns at 800 ° C and 25 ° C post in-situ, and the monoclinic α'-Ga_2S_3 phase (JCPDS no. 01-076-0752).

4. Conclusion

Ga_2S_3 samples have been prepared by mechanical alloying of pure raw Ga and S and the mechanism of reactivity has been investigated. Our work shows that after only 1 h of milling, the main phases identified are monoclinic α'-Ga_2S_3 and GaS, that further react to form Ga_2S_3 in 4 h. It is therefore a fast and energy-efficient synthesis technique compared to melt quenching process performed at high temperature (above 1180 °C). Moreover, the evolution of the color as the synthesis progresses allows a simple and direct follow-up of the reaction progress. The XRD studies and the Rietveld refinements also show that the material mechano-synthesized is a mixture of phases: a majority hexagonal β phase (68% ± 5%) and a cubic γ phase (32% ± 5%). The high temperature XRD analysis reveals that no evolution of the two phases occurs before a phase transition to monoclinic α' starting at 450°C. Furthermore, the relative amount of the two phases can be modify by the quantity of precursors added. This work provides new insight in the reactivity of Ga and S mixtures, and shows that structural modifications accessible by mechanical synthesis can be different than by traditional melting-quenching method in silica tube. Finally, the main advantage of this synthesis technique is that a large quantity of Ga_2S_3 can be produced in a short time at a very low cost. This efficient process is interesting for all applications that do not need a specific polymorph of Ga_2S_3 as a starting material such as gigahertz and terahertz applications, or glasses for optics and solar panels.

AUTHOR INFORMATION

Corresponding Authors

Louisiane Verger - Univ Rennes CNRS, ISCR (Institut des Sciences Chimiques de Rennes) - UMR 6226, F-35000 Rennes, France ; Email : louisiane.verger@univ-rennes1.fr

Laurent Calvez - Univ Rennes CNRS, ISCR (Institut des Sciences Chimiques de Rennes) - UMR 6226, F-35000 Rennes, France ; Email : laurent.calvez@univ-rennes1.fr

Notes

The authors declare no competing financial interest.

ACKNOWLEDGMENTS

Authors would like to acknowledge the IUF (Institut Universitaire de France) for their financial support.

REFERENCES

[1] K. Wang, W. Ye, W. Yin, W. Chai, Y. Rui, B. Tang, A novel carbon-coated Ga_2S_3 anode material derived from post-synthesis modified MOF for high performance lithium ion and sodium ion batteries. *Electrochimica Acta*. **2019**, 322, 134790.

[2] S. Cozic, A. Bréhault, and D. Le Coq, GeS_2–Ga_2S_3–LiCl Glass System: Electrical Conductivity and Structural Considerations. *International Journal of Applied Glass Science*. **2016**, 7 (4), 513–523.

[3] A. Paraskiva, M. Bokova, E. Bychkov, Na^+ ion conducting glasses in the NaCl-Ga_2S_3-GeS_2 system: A critical percolation regime. *Solid State Ionics*, **2017**, 299, 2–7.

[4] H. Senoh, H. Kageyama, T. Takeuchi, K. Nakanishi, T. Ohta, H. Sakaebe, M. Yao, T. Sakai, K. Yasuda, Gallium (III) sulfide as an active material in lithium secondary batteries. *Journal of Power Sources*, **2011**, 196 (13), 5631–5636/

[5] P. Wang, M. Liu, F. Mo, Z. Long, F. Fang, D. Sun, Y. Zhou and Y. Song, Exploring the sodium ion storage mechanism of gallium sulfide (Ga_2S_3): a combined experimental and theoretical approach. *Nanoscale*, **2019**, 11 (7), 3208–3215.

[6] Z. M. Hu, G. Tao Fei, L. D. Zhang, Synthesis and tunable emission of Ga_2S_3 quantum dots. *Materials Letters*, **2019**, 239, 17–20.

[7] V. Seznec, H.L. Ma, X.H. Zhang, V. Nazabal, J.L. Adam, X.S. Qiao, X.P. Fan, Preparation and luminescence of new Nd^{3+} doped chloro-sulphide glass–ceramics. *Opt. Mater.*, **2006**, 29 (4), 371-376.

[8] C. Lin, L. Calvez, Z. Li, S. Dai, H. Tao, H. Ma, X. Zhang, B. Moine, and X. Zhao, Enhanced Up-Conversion Luminescence in Er^{3+}-Doped 25GeS_2-35Ga_2S_3-40CsCl Chalcogenide Glass–Ceramics. *J. Am. Ceram. Soc*., **2013**, 96 (3), 816–819.

[9] S.P. Morgan, D. Furniss, A.B. Seddon, Lanthanum-fluoride addition to gallium-lanthanum-sulphide. *Journal of Non-Crystalline Solids*, **1996**, 203, 135-142.

[10] M.T. de Araujo, J.A. Medeiros Neto, A.S.B. Sombra, A.S. Oliveira, A.S. Gouveia-Neto, Multiwavelength frequency-doubling in bulk gallium-lanthanum-sulphide glasses for optical fiber amplifiers at 1.3μm, *Optical Materials*, **1997**, 7 (1-2), 1-7.

[11] I.V. Kityk, V.V. Halyan, V.O. Yukhymchuk, V.V. Strelchuk, I.A. Ivashchenko,Ya. Zhydachevskyy, A. Suchocki, I.D. Olekseyuk, A.H. Kevshyn, M. Piaseckia, NIR and visible luminescence features of erbium doped Ga_2S_3–La_2S_3 glasses. *Journal of Non-Crystalline Solids*, **2018**, 498, 380–385.

[12] O.V. Tsisar, L.V. Piskach, O.V. Parasyuk, et al., Tl_2S–Ga_2S_3–GeS_2 glasses for optically operated laser third harmonic generation. *J. Mater. Sci. Mater. Electron*., **2017**, 28 (24), 19003.

[13] J. Ebothe, K.J. Plucinski, W. Imiolek, $GeSe_2$–Ga_2S_3–PbI_2 glass alloys like second-order non-linear optical materials. *Journal of Alloys and Compounds*, **2008**, 456 (1-2), 27–29.

[14] P. Masselin, D. Le Coq, L. Calvez, E. Petracovschi, E. Lépine, E. Bychkov, X. Zhang, CsCl effect on the optical properties of the $80GeS_2$–$20Ga_2S_3$ base glass. *Appl. Phys. A*, **2012**, 106 (3), 697–702.

[15] C. Lin, L. Calvez, B. Bureau, H. Tao, M. Allix, Z. Hao, V. Seznec, X. Zhang, and X. Zhao, Second-order optical nonlinearity and ionic conductivity of nanocrystalline GeS_2–Ga_2S_3–LiI glass-ceramics with improved thermo-mechanical properties. *Phys. Chem. Chem. Phys*., **2010**, 12 (15), 3780–3787.

[16] A.F. Qasrawia, Olfat A. Omareya, Characterization of the Al/Ge/In_2Se_3/Ga_2S_3/Al hybrid tunneling barriers designed for Gigahertz/Terahertz applications. *Thin Solid Films*, **2018**, 660, 276–281.

[17] S. E. Al Garni, A. F. Qasrawi, Tunable Au/Ga_2S_3/Yb Varactor Diodes Designed for High Frequency Applications. *Chalcogenide Letters*, **2017**, 14 (9), 381-388.

[18] N. Zhou, L. Gan, R. Yang, F. Wang, L. Li, Y. Chen, D. Li, and T. Zhai, Nonlayered Two-Dimensional Defective Semiconductor γ- Ga_2S_3 toward Broadband Photodetection. *ACS Nano*, **2019**, 13 (6), 6297−6307.

[19] M. M. Y. A. Alsaif, N. Pillai, S. Kuriakose, S. Walia, A. Jannat, K. Xu, T. Alkathiri, M. Mohiuddin, T. Daeneke, K. Kalantar-Zadeh, J. Z. Ou, and A. Zavabeti, Atomically Thin Ga_2S_3 from Skin of Liquid Metals for Electrical, Optical, and Sensing Applications, ACS Appl. Nano Mater., **2019**, 2 (7), 4665−4672.

[20] Y. Wei, D. Zhuang, M. Zhao, N. Zhang, X. Yuc, X. Li, X. Lyu, C. Wang, L. Hu, Fabrication of in-situ Ti-doped CuGaS2 thin films for intermediate band solar cell applications by sputtering with $CuGaS_2$:Ti targets. *Vacuum*, **2019**, 169, 108921.

[21] L. Hu, and D. Wei, Janus Group-III Chalcogenide Monolayers and Derivative Type-II Heterojunctions as Water-Splitting Photocatalysts with Strong Visible-Light Absorbance. *J. Phys. Chem. C,* **2018**, 122 (49), 27795−27802.

[22] M. Guymont, A. Tomas, M.-P. Pardo, and M. Guittard. Electron Microscope Study of γ-Ga_2S_3. *Phys. Stat. Sol. (a)*, **1989**, 113 (1), K5-K7.

[23] A. Tomas, M. Guymont, M. P. Pardo, M. Guittard, and J. Flahaut. X-Ray Diffraction and Electron Microscopy Studies of α- and β-Ga_2S_3. *Phys. Stat. Sol. (a)*, **1988**, 107, 775-784.

[24] A. Neuhaus, M. Kaempffer. Studies on the binary system zinc sulfide-gallium sesquisulfide at pressures up to 150 kbars and temperature T = 800°. *Neues Jahrb. Mineral.,* **1981**, 141, 186-200.

[25] A. Tomas, M.P. Pardo, M. Guittard, M. Guymont, R. Famery. Détermination des structures des formes α et β de Ga_2S_3, structural determination of α and β Ga_2S_3. *Mater. Res. Bull.*, **1987**, 22 (11), 1549-1554.

[26] G. Collin, J. Flahaut, M. Guittard and A-M. Loireau-Lozach. Préparation et Structure de Ga_2S_3 α Type Wurtzite Lacunaire. *Mat. Res. Bull.*, **1976**, 11 (3), 285-292.

[27] M. P. Pardo, M. Guittard, A. Chilouet, et A. Tomas. Diagramme de phases gallium-soufre et études structurales des phases solides. *J. Sol. Stat. Chem.*, **1993**, 102 (2), 423-433.

[28] M.P. Pardo, A. Tomas et M. Guittard. Polymorphism of Ga_2S_3 and Phase Diagram of Ga-S. *Mat. Res. Bull.*, **1987**, 22 (12), 1677-1684.

[29] H. Hahn et G. Frank. Zur Struktur des Ga_2S_3. *Z. anorg. Chem*., **1955**, 278 (5-6), 333-339.

[30] J. Goodyear, W.J. Duffin et G.A. Steigman. The unit cell of α-Ga_2S_3. *Acta Cryst*., **1961**, 14 (11), 1168-1170.

[31] A. Zavrazhnov, S. Berezin, A. Kosykov et al. The phase diagram of the Ga–S system in the concentration range of 48.0–60.7 mol% S. *J Therm. Anal. Calorim*, **2018**, 134 (1), 483–492.

[32] A. Brukl et G. Ortner, G. Die Sulfide des Galliums. *Naturwissenschaften*, **1930**, 18, 393.

[33] H. Hahn et W. Klingler. Über die Kristallstrukturen von Ga_2S_3, Ga_2Se_3 und Ga_2Te_3. *Z. anorg. Chem.*, **1949**, 259 (1-4), 135-142.

[34] T. Ahamad and S. M Alshehri, Green Synthesis and Characterization of Gallium (III) Sulphide (α-Ga_2S_3) Nanoparicles at Room Temperature. *Nano Hybrids*, **2014**, 6, 37-46.

[35] S. A. Alderhami, D. Collison, D. J. Lewis, P. D. McNaughter, P. O'Brien, B. F. Spencer, I. Vitorica-Yrezabala and G. Whitehead. Accessing γ-Ga_2S_3 by solventless thermolysis of gallium xanthates: a low-temperature limit for crystalline products. *Dalton Trans.*, **2019**, 48 (41), 15605-15612.

[36] M. Kristl, S. Gyergyek, N. Srt, and I. Ban. Mechanochemical Route for the Preparation of Nanosized Aluminum and Gallium Sulfide and Selenide. *Materials and Manufacturing Processes*, **2016**, 31 (12), 1608–1612.

[37] P. Baláž, M. Achimovičová, M. Baláž, P. Billik, Z. Cherkezova-Zheleva, J. Manuel Criado, F. Delogu, E. Dutková, E. Gaffet, F. José Gotor, R. Kumar, I. Mitov, T. Rojac, M. Senna, A. Streletskii and K. Wieczorek-Ciurowa. Hallmarks of mechanochemistry: from nanoparticles to technology. *Chemical Society. Reviews*, **2013** ,42, 7571-7637.

[38] M. Baláž, P. Baláž, M. J. Sayagués, A. Zorkovská. Bio-inspired mechanochemical synthesis of semiconductor nanomaterial using eggshell membrane. *Materials Science in Semiconductor Processing*, **2013**, 16 (6), 1899–1903.

[39] J. Wang, Q. Zhang, F. Saito. Improvement in the floatability of CuO by dry grinding with sulphur. *Colloids and Surfaces A: Physicochemical and Engineering Aspects*, **2007**, 302 (1-3), 494–497.

[40] W. Yuan, J. Li, Q. Zhang, and F. Saito. Mechanochemical sulfidization of lead oxides by grinding with sulfur. *Powder technology*, **2012**, 230, 63-66.

[41] E. Boldyreva. Mechanochemistry of inorganic and organic systems: What is similar, what is different? *Chemical Society Reviews*, **2013**, 42 (18), 7719–7738.

[42] P.Baláž, M. Baláž, M. Achimovičová, Z. Bujňáková, and E. Dutková. Chalcogenide mechanochemistry in materials science: insight into synthesis and applications (a review). *Journal of Materials Science*, **2017**, 52 (20), 11851-11890.

[43] M. Baláž, A. Zorkovská, F. Urakaev, P. Baláž, J. Briančin, Z. Bujňáková, E. Gock. Ultrafast mechanochemical synthesis of copper sulfides. *RSC Advances*, **2016**, 6 (91), 87836-87842.

[44] J. Rodríguez-Carvajal. Recent advances in magnetic structure determination by neutron powder diffraction. *Physica B: Condensed Matter*., **1993**, 192 (1-2), 55–69.

[45] T. Roisnel, J. Rodriguez-Carvajal. WinPLOTR: A Windows tool for powder diffraction pattern analysis. *Mater. Sci. Forum: European Powder Diffraction EPDIC7*, **2001**, 378 (1), 118-123.

GRAPHICAL ABSTRACT